IET Microwaves, Antennas & Propagation

Research Article

IET Journals
The Institution of Engineering and Technology

Decoupling using diamond-shaped patterned ground resonator for small MIMO antennas

ISSN 1751-8725
Received on 17th May 2016
Revised on 28th June 2016
Accepted on 14th July 2016
doi: 10.1049/iet-map.2016.0400
www.ietdl.org

Di Wu ✉, *Sing Wai Cheung*, *Qin Long Li*, *Tung Ip Yuk*

Department of Electrical and Electronic Engineering, The University of Hong Kong, Hong Kong, People's Republic of China
✉ *E-mail: diwu@eee.hku.hk*

Abstract: A decoupling technique using a patterned ground structure for small multiple-input multiple-output (MIMO) antennas is proposed in this study. The MIMO antenna consists of two symmetrical L-shaped inverted-F antenna (IFA) elements designed to operate in the wireless-local-area-network band and installed on a compact printed-circuit board (PCB) with a size of 72.4×20 mm^2 serving as ground. The two IFA elements have a very short separating distance of only 16.2 mm (0.13λ). To reduce strong mutual coupling, a diamond-shaped patterned ground resonator (DSPGR) with a compact size of 16.2×10.13 mm^2 is printed on the PCB between the two IFA elements. The effect of the DSPGR on reducing mutual coupling is studied using computer simulation. The impedance bandwidth, mutual coupling, peak gain, radiation pattern and efficiency, envelope-correlation coefficient and multiplexing efficiency of the MIMO antenna are studied using simulation and measurement. Results show that the DSPGR can dramatically reduce mutual coupling between the two IFA elements to below −20 dB within the operating frequency range of 2.18–2.65 GHz (19.5%).

1 Introduction

With the ever-increasing demand for higher data rates, multiple-input multiple-output (MIMO) technology has become one of the core technologies for the current 4G and future 5G wireless telecommunication standards. By utilising the spatial degree of freedom in wireless multipath channels, MIMO antennas can be used to improve data throughput and channel capacity of communications systems without requiring additional frequency spectrum or transmit power [1]. However, to achieve the promises of MIMO technology, one of the key requirements is to have sufficiently high isolation (or low mutual coupling or correlation) between antenna elements in the MIMO antennas installed at the transmitters and receivers of communications systems [2]. Theoretically, adjacent antenna elements in a MIMO antenna can be placed at a distance of about $\lambda/2$ to minimise mutual coupling and signal correlation [3]. For small mobile terminals where space for antenna installation is very limited, it is very difficult to satisfy the criterion of $\lambda/2$-distance separation for MIMO antennas. Thus developing novel and effective decoupling techniques for MIMO antennas used in small mobile terminals is always a hot topic.

In the past, different decoupling techniques such as decoupling networks [4–7], electromagnetic bandgap (EBG) structures [8, 9] and metamaterials [10–12], defected-ground structures (DGS) [13–15], parasitic elements [16–20], and neutralisation-line techniques [21, 22] have been reported. In [4], series/shunt reactive elements were added to each port for port decoupling. Although this method could reduce mutual coupling between antenna elements of a MIMO antenna from −3 to −20 dB, the decoupling bandwidth was quite narrow from 2.4 to 2.5 GHz. Moreover, the reactive elements would give rise to extra power dissipation when the MIMO antenna was operating in the higher frequency bands. In [6, 7], eigenmode feeding networks using 90°/180°-hybrid couplers were used to reduce mutual coupling in MIMO antennas. The feeding networks were too large to be used with compact MIMO antennas, and insertion losses of the complicated networks led to low antenna efficiencies. In [8–12], mushroom-like EBG structures and metasurface (MS) were inserted between the antenna elements of MIMO antennas to suppress surface-wave propagation and achieve lower mutual coupling. The EBG structures and MS were too large and complicated to be fabricated. In [13], a DGS structure with fish-bone-like slots was etched on the ground plane between two planar-inverted-F antennas (PIFAs), and the bandstop-filter effect of the slots in the DGS structure prevented coupling current from flowing on the ground. A large ground plane was needed for the slots to have sufficient isolation. For compact MIMO antenna design, parasitic elements and neutralisation-line methods are used quite often. In [16–20], a parasitic element was inserted between antenna elements to artificially create an additional coupling path to reduce coupling. This method was applied to a 2.4-GHz USB dongle antenna in [16], a mobile antenna in [18], and the UWB antennas in [19, 20]. However, the decoupling bandwidth for $S_{21} < -20$ dB was limited [16], or mutual coupling could not reach below −20 dB [18, 19]. Neutralisation-line technique requires a suspended line physically connected between two antenna elements. The neutralisation line generates another current path to cancel out mutual coupling. However, as shown in [21, 22], the decoupling bandwidths were quite limited.

It is well known that we can design a bandstop resonator on the ground plane using patterned ground structures (a type of DGSs) to suppress signals from going through a microstrip line [23, 24]. In this paper, we propose to employ a patterned ground structure to reduce mutual coupling of two symmetrical L-shaped inverted-F antenna (IFA) elements in a small MIMO antenna. The patterned ground structure has a diamond shape and serves as a resonator, so it is here called a diamond-shaped patterned ground resonator (DSPGR). To the best knowledge of the authors, the proposed DSPGR decoupling structure has never been used in decoupling of antenna elements in MIMO antennas. Results show that the DSPGR can significantly reduce mutual coupling across a wide bandwidth by suppressing the surface currents between the two antenna elements of the MIMO antenna. Compared with the previous decoupling techniques in [4–6, 8–13, 16, 21], with the given impedance bandwidth (IMBW) and decoupling bandwidth, the proposed DSPGR can lead to a much more compact antenna size of $0.094\lambda^2$, where λ is the free space wavelength. The preliminary study using computer simulation on the design was reported by the authors in [25], which only illustrated the basic effects. In this paper, a detailed study is carried out on the same MIMO antenna using the EM simulation tool CST and the antenna measurement equipment, the Satimo StarLab system. The MIMO

antenna is designed to operate in the WLAN band and has an operating frequency range of 2.18–2.65 GHz. The two IFA elements are separated by a patterned ground structure similar to the one in [24], but not on a microstrip line. The simulated and measured S_{11}, S_{21}, radiation patterns, efficiencies, realised peak gains, envelope-correlation coefficients (ECCs) of the MIMO antenna are also presented. Comparison with other designs is also made.

2 MIMO antenna design

The proposed compact MIMO antenna used for study, as shown in Fig. 1, is designed on a single-sided PCB with an area of $l \times w = 72.4 \times 20$ mm^2 serving as ground. Two symmetrical L-shaped IFA elements (denoted here as IFAs #1 and #2 in Fig. 1*a*) installed on the ground plane serving as radiators. The shorting pins of the IFA elements are directly soldered on the ground plane and ports #1 and #2 are for feeding the input signal to the antenna. The IFA elements have a height of $h = 6$ mm, a width of $w_4 = 1$ mm and a length of $l_3 + l_4 = 7.5 + 19$ mm $= 26.5$ mm, equivalent to about $\lambda/4$, where λ is the free space wavelength at 2.45 GHz in the WLAN band. It should be noted that, although the MIMO antenna is set to operate in the WLAN band, it can set using l_3 to operate within the frequency range of 2.18–2.65 GHz, as will be shown later. The

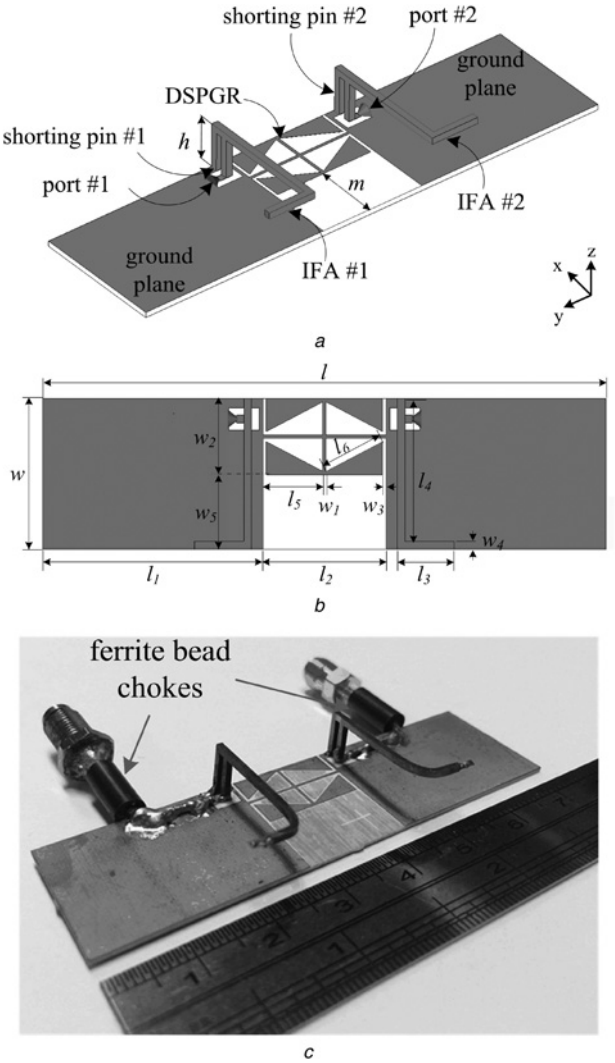

Fig. 1 *Geometry and dimensions of proposed MIMO antenna*

a 3D view
b 2D top view
c Prototyped MIMO antenna

Table 1 Dimensions of proposed MIMO antenna (mm)

l	l_1	l_2	l_3	l_4	l_5	l_6
72.4	29	16.2	7.5	19	7.88	8.4
w	w_1	w_2	w_3	w_4	w_5	h
20	0.45	10.13	0.45	1	9.87	6

two IFA elements are separated at a very short distance of $l_2 = 16.2$ mm, equivalent to only about 0.13λ, much less than the distance of 0.5λ (61 mm) required for minimum mutual coupling [3]. To reduce strong mutual coupling at such a short distance, the copper layer with an area of $w \times l_2 = 20 \times 16.2$ mm between the two IFA elements on the ground plane is removed, as shown in Fig. 1*b*, and replaced by a patterned ground structure having a rectangular shape of $w_2 \times l_2 = 10.13 \times 16.2$ mm^2 with a diamond-shaped slot in the middle. Two conducting traces with a width of $w_1 = 0.45$ mm, forming a '+' sign, are used to connect together the opposite vertices of the diamond-shaped slot. Thus the left and right portions of the ground plane are connected together by the horizontal conducting trace. The structure is similar to the compact microstrip resonant cell in [24] used on a microstrip line to stop current from passing through, but the proposed structure here is used on the ground plane without having a microstrip line. Since the diamond-shaped patterned ground structure is a bandstop resonator, it is here called a diamond-shaped patterned-ground resonator (DSPGR). It will show later that the DSPGR can suppress the surface-current flow between the two IFA elements in the 2.4-GHz WLAN band. The EM simulation tool CST is used to study and design the MIMO antenna on a Rogers substrate, RO4350B, with a thickness of 0.8 mm, a relative permittivity of 3.48 and a loss tangent of 0.0037. Detailed dimensions of the design are listed in Table 1, which is used to fabricate the prototyped MIMO antenna shown in Fig. 1*c* for measurement using the antenna measurement system, Satimo Starlab system.

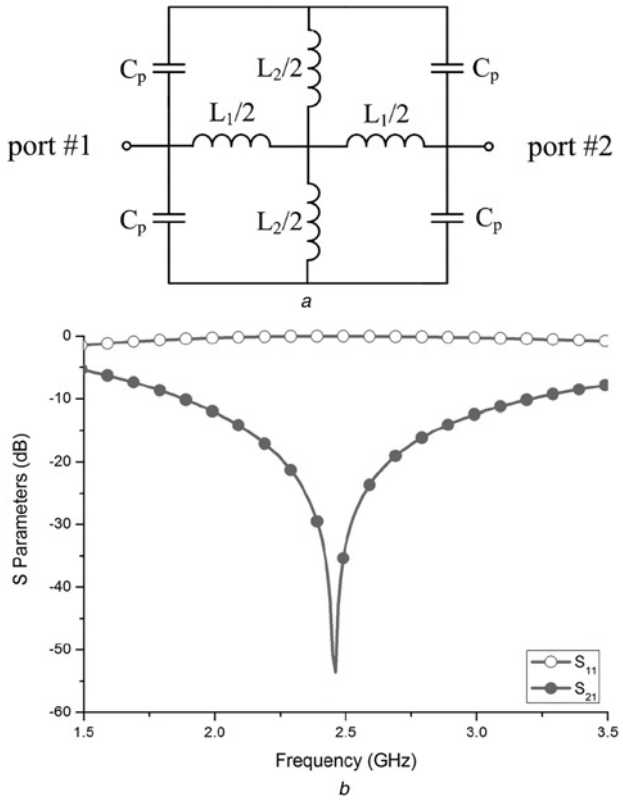

Fig. 2 *DSPGR*

a LC equivalent-circuit model
b S_{11} and S_{21} of equivalent-circuit model with $L_1 = 10.5$ nH, $L_2 = 6.5$ nH and $C_p = 0.4$ pF

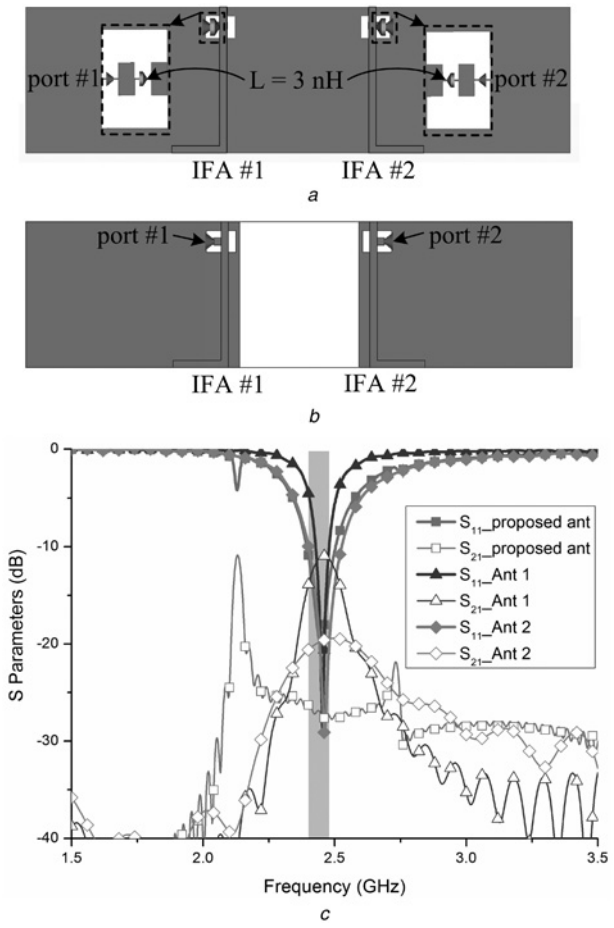

Fig. 3 *Two antenna used for comparison*

a Ant 1
b Ant 2
c Simulated S_{11} and S_{21} of proposed MIMO antenna, Ant 1 and Ant 2

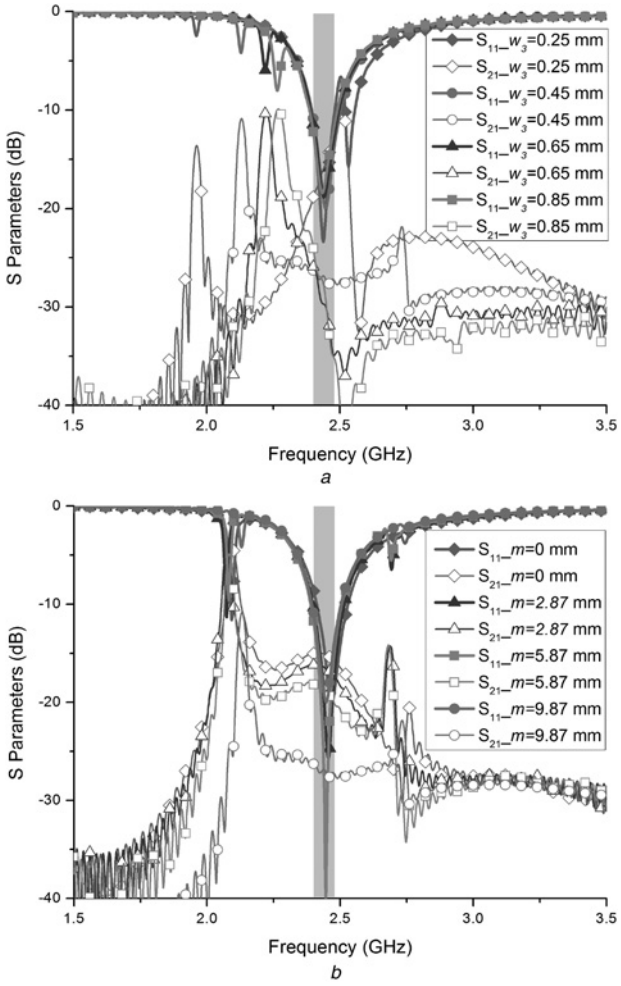

Fig. 5 *Parameter study of DSPGR*

a Simulated S_{11} and S_{21} with different values of w_3 in MIMO antenna
b Simulated S_{11} and S_{21} with different values of m in MIMO antenna

In simulation, no feeding cable is required to feed the input signal to the antenna. However, in measurement, a feeding cable is needed to connect the antenna to the antenna measurement system. When the ground plane is electrically small as in the proposed MIMO antenna, current will flow back from the antenna ground plane to the outer surface of the feeding cable, resulting in radiation [26]. This cable effect will affect the accuracy of the measured radiation patterns. To reduce the cable effect in measurement, we employ two ferrite bead chokes, as shown in Fig. 1*c*, at the input ports of the MIMO antenna. The ferrite bead has a very high permeability, which can absorb the current flowing back from the antenna, hence resulting in more accurate measured radiation patterns. However, as some power is absorbed by the ferrite bead chokes, the measured efficiency and gain will be less than the actual values as shown later.

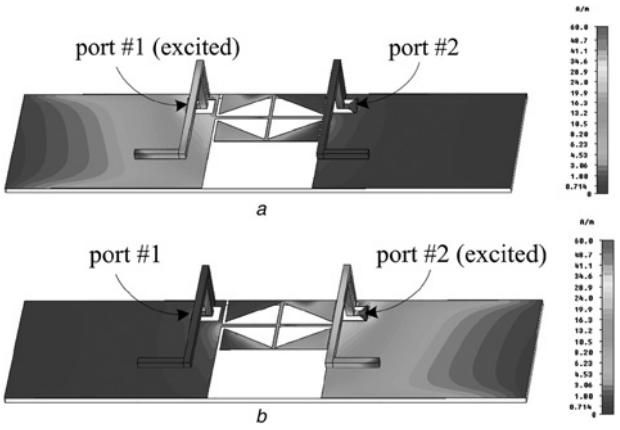

Fig. 4 *Current distribution at 2.45 GHz*

a Port #1 excited
b Port #2 excited

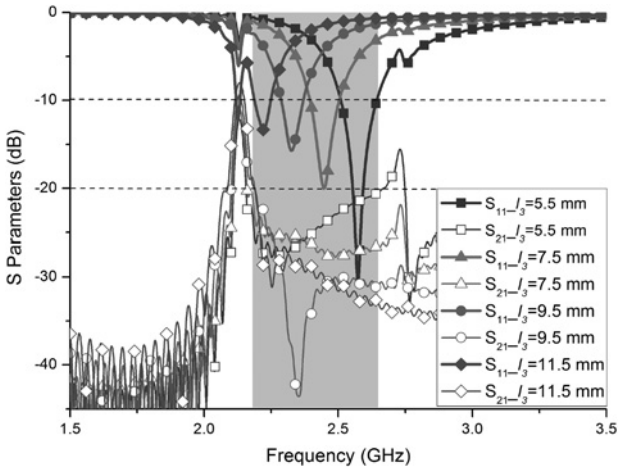

Fig. 6 *Simulated S_{11} and S_{21} with different lengths of l_3 in MIMO antenna*

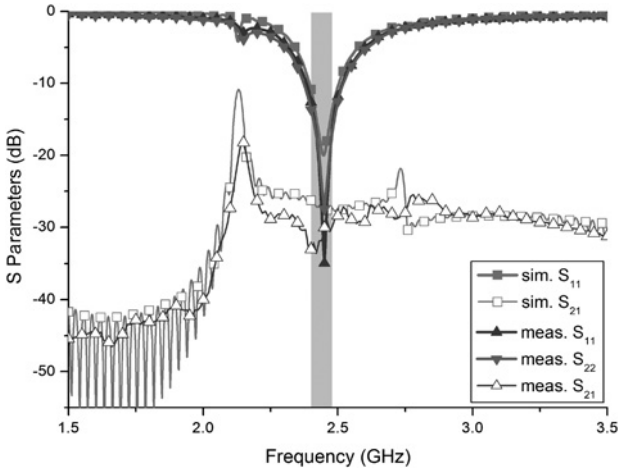

Fig. 7 *Simulated and measured S_{11} and S_{21} of MIMO antenna*

3 Study of antenna

3.1 Equivalent circuit model of DSPGR

The DSPGR in Fig. 1 can be modelled using a simple LC equivalent-circuit model shown in Fig. 2*a*, where L_1 represents the total series inductance introduced by the horizontal trace, L_2 represents the total series inductance introduced by the vertical trace, and C_p represents the series capacitance introduced by the triangular slots and the gaps W_3 between the DSPGR and the ground plane. It should be noted that the equivalent circuit is similar to but not the same as the one in [24]. The difference is that there is no ground plane underneath the DSPGR, so the capacitance (C_0 used in [24]) between the triangular patch and the ground plane does not exist. Computer simulation using the Advanced Design System (ADS) has shown that the equivalent-circuit model shown in Fig. 2*a* is indeed a bandstop filter. For example, with $L_1 = 10.5$ nH, $L_2 = 6.5$ nH, $C_p = 0.4$ pF, the simulated S_{11} and S_{21} of the circuit shown in Fig. 2*b* indicates that the circuit has a resonance at 2.45 GHz, a stopband from 2.27 to 2.66 GHz and mutual coupling between ports #1 and #2 of less than 20 dB, as indicated by S_{21}.

3.2 Effects of DSPGR on reducing mutual coupling

To study the effects of the DSPGR on reducing mutual coupling, we compare it with two similar antennas: (i) Ant 1 having a plain copper plate to replace the DSPGR as shown in Fig. 3*a*, and (ii) Ant 2 having the DSPGR removed as shown in Fig. 3*b*. For Ant 1, since the DSPGR is removed, simulation has shown that an impedance matching network using a series chip inductor $L = 3$ nH, as shown in Fig. 3*a*, is required for good matching. The simulated S_{11} and S_{21} of the three antennas and the proposed MIMO antenna are all shown in Fig. 3*d* for comparison. In the figure, S_{11} and S_{21} of the same antenna are shown by the thick and thin curves, respectively, of the same colour. It can be seen that all antennas have the resonances at around 2.45 GHz. With using the DSPGR, the proposed MIMO antenna has an IMBW, for $S_{11} < -10$ dB, of 2.4–2.48 GHz, enough to cover the 2.4-G WLAN band. Mutual coupling between the two input ports is −27.6 dB at 2.45 GHz, as indicated by S_{21}. When the DSPGR is replaced by a simple ground plane as in Ant 1, surface currents can directly propagate through the ground plane between the two IFAs, so mutual coupling increases from −27.6 to −11 dB by 16.6 dB at 2.45 GHz, as shown in Fig. 3*d*. The IMBW reduces to 2.43–2.48 GHz, which cannot cover the 2.4-GHz WLAN system. When the DSPGR is removed from the proposed MIMO antenna as in Ant 2, compared with Ant 1, surface currents between the two IFA elements are substantially reduced, so mutual coupling reduces from −11 to −19.7 dB by about 8 dB at 2.45 GHz, which is still 8 dB higher

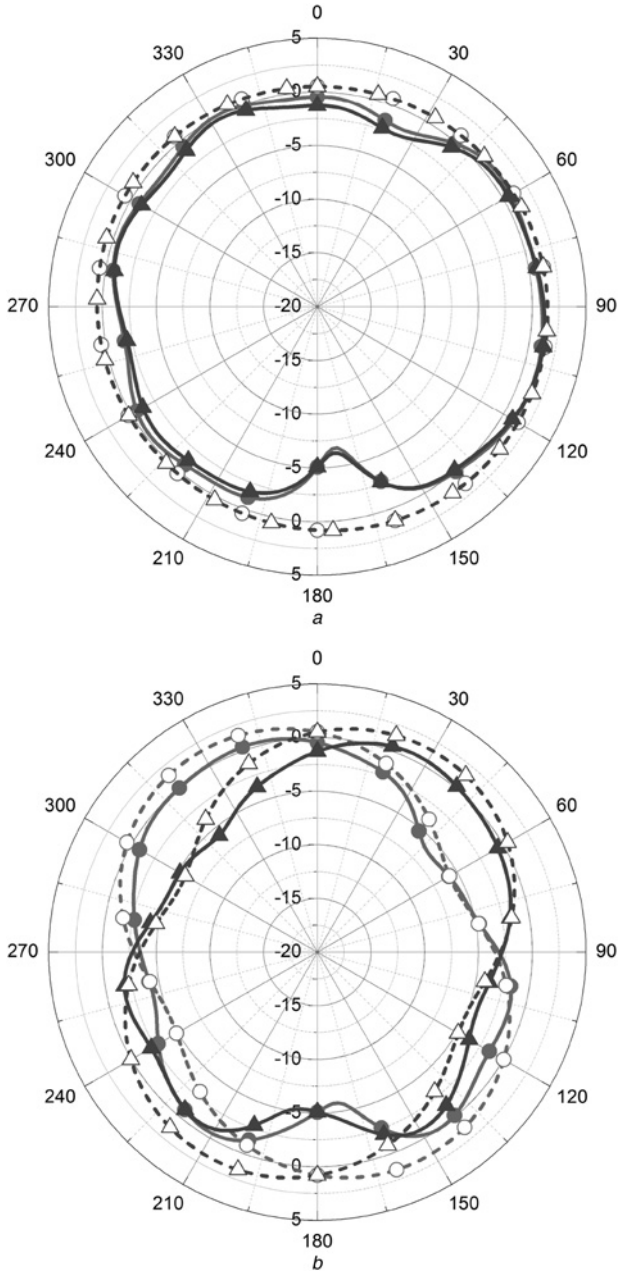

Fig. 8 *Simulated and measured radiation patterns at 2.45 GHz*

(Line with a open circle indicates sim. pattern of antenna #1; line with a filled circle indicates meas. pattern of antenna #1; line with a white up-pointing triangle indicates sim. pattern of antenna #2; and line with a black up-pointing triangle indicates meas. pattern of antenna #2)

a *x*–*z* plane

b *y*–*z* plane

than that of the proposed MIMO antenna. The IMBW bandwidth increased slightly to 2.4–2.53 GHz. All these results show that the DSPGR can effectively reduce mutual coupling between the two IFA elements by suppressing surface currents propagation.

3.3 Surface current analysis

The decoupling effect of the DSPGR is further studied using current distribution. Fig. 4 shows the simulated current distribution of the MIMO antenna at 2.45 GHz. With port #1 is excited and port #2 terminated with a 50-Ω load, Fig. 4*a* shows that the current is mainly concentrated in the region close to the feed point of IFA #1. The current on the right-hand portion of the ground plane remains very weak. This is because the DSPGR suppresses the

IET Microw. Antennas Propag., 2017, Vol. 11, Iss. 2, pp. 177–183

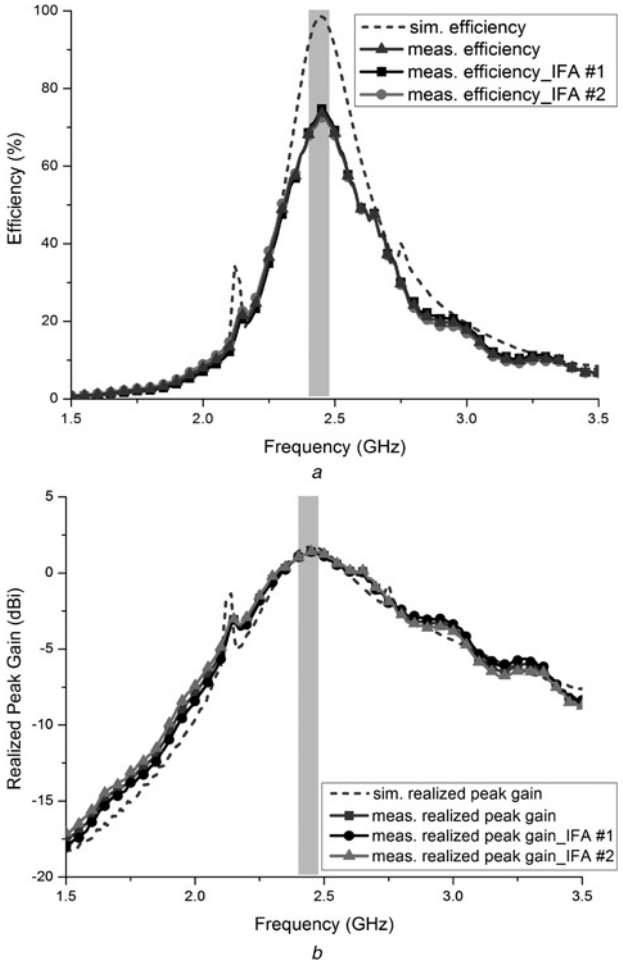

Fig. 9 *Simulated and measured radiation performances of MIMO antenna*
a Efficiencies
b Realised peak gains

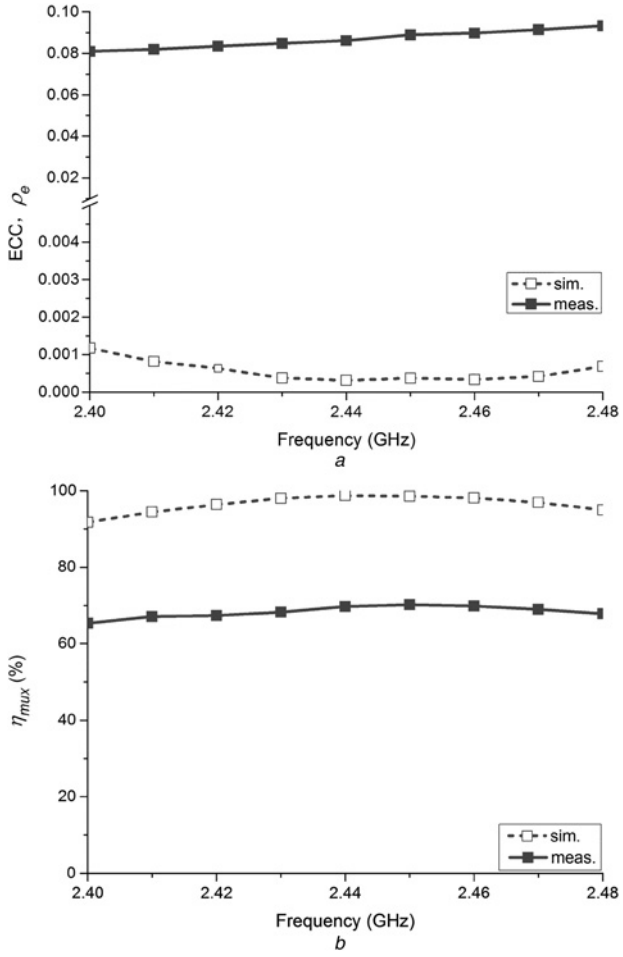

Fig. 10 *Simulated and measured diversity performances of MIMO antenna*
a ECC (ρ_e)
b Multiplexing efficiency (η_{mux})

surface current travelling from port #1 to port #2. The same phenomenon is observed in Fig. 4*b* when port #2 is excited and port #1 is terminated with a 50-Ω load.

3.4 Parameter study of DSPGR

The DSPGR has a number of parameters, which can affect the decoupling performance. However, simulation studies have shown that the parameters w_3 (the gap between the DSPGR and the ground plane) and m (distance between the edge of the DSPGR and the edge of the PCB, as shown in Fig. 1*a*) are most important for the design of the MIMO antenna, so parameter studies are carried out on these parameters.

The simulated S_{11} and S_{21} of the MIMO antenna with different values of w_3 are shown in Fig. 5*a*. In the study, dimension l is kept constant, so the overall size of the antenna is not changed. It can be seen that, varying w_3 has little effects on the main resonant frequency of 2.45 GHz. With w_3 decreased from 0.85 to 0.25 mm, leading to larger capacitances in the equivalent-circuit model of Fig. 2*a*, the S_{21} curves shift to low frequencies. As far as the 2.4-GHz WLAN band is concerned, the worst case is $w_3 = 0.25$ mm when mutual coupling (as indicated by S_{21}) increases to about −12 dB. With w_3 increased to 0.45 mm, mutual coupling is quite constant at below −20 dB from 2.16 to 2.72 GHz (22.2%), which can cover the 2.4-GHz WLAN band. Thus the gap dimension w_3 can be used to adjust the frequency band for minimising mutual coupling.

The parameter m is the distance between the edge of the DSPGR and the edge of the PCB as shown in Fig. 1*a*. With $m = 9.87$, the edge of the DSPGR is alighted with the edge of the PCB as shown in Fig. 1*a*. As m decreases, the DSPGR moves toward the other side of the PCB, so m determines the location of the DSPGR on the substrate. The simulated S_{11} and S_{21} with different values of m are shown in Fig. 5*b*. It can be seen that, as m decreases from 9.87 to 5.87, 2.87, and 0 mm, mutual coupling at 2.45 GHz increases from −27 dB to −19, −16.7, and −15 dB, respectively. Thus the DSPGR is most effectively with $m = 9.87$, i.e. when located next to the feed points where current is the strongest. Note that the value of m does not affect the IMBW of the antenna, as indicated in Fig. 5*b*.

4 Simulation and measurement results

4.1 Operating frequency range

The lengths ($l_3 + l_4$) and heights (h) of the radiators in IFAs #1 and #2 determine the operating frequency of the MIMO antenna. In the current design, l_4 and h are fixed, so only l_3 can be used to set the operating frequency. Here we study the operating frequency range of the MIMO using l_3. Fig. 6 shows the simulated S_{11} and S_{21} with different values of l_3. Again, in the figure, S_{11} and S_{21} are shown by the thick and thin curves, respectively, of the same value of l_3. It can be seen that with $l_3 = 5.5$, 7.5, 9.5 and 11.5 mm, the resonant frequencies are 2.58, 2.45, 2.33 and 2.22 GHz, respectively. However, l_3 also affects mutual coupling of the antenna. It can be seen that the antenna has $S_{11} < -10$ dB and $S_{11} < -20$ when l_3 is in the range of 5.5 mm $< l_3 <$ 11.5 mm or when the frequency band is within the range of 2.18–2.65 GHz (19.5%), as shown in the grey zone of Fig. 6. Thus the MIMO antenna can be used for any systems operating within the frequency range of 2.18–2.65 GHz for

Table 2 Comparison with other decoupling methods

Reference	Method	Centre frequency	IMBW, GHz ($S_{11} \leq -10$ dB)	Isolation level	Decoupling bandwidth ($S_{21} \leq -20$ dB)	Antenna spacing, mm (edge to edge)	Decoupling structure size	Total size
[4]	LC port decoupling network	2.45	2–2.51 (22.6%)	22 dB (improved by 19 dB)	2.45–2.48 GHz (1.2%)	8.5 (0.069λ)	≃8.5 × 2 mm^2 (0.00113λ^2)	78 × 22 mm^2 (0.115λ^2)
[5]	coupled resonator decoupling network	2.62	2.46–2.78 (10.3%)	25 dB	2.5–2.77 GHz (15%)	9.8 (0.084λ)	12.35 × 9.5 mm^2 (0.009λ^2)	>54 × 72 mm^2 (0.299λ^2)
[6]	180°/90° couplers for eigenmode decoupling	2.6	2.56–2.6 (1.6%)	23 dB	–	11.5 (0.1λ)	115 × 115 mm^2 (1λ^2)	115 × 115 mm^2 (1λ^2)
[8]	EBG structure	5.85	5.8–5.9 (1.7%)	25 dB (improved by 8 dB)	–	38.8 (0.75λ)	47.5 × 13.5 mm^2 (0.247λ^2)	100 × 50 mm^2 (1.922λ^2)
[9]	UC-EBG structure	5.75	5.7–5.82 (2%)	25 dB (improved by 10 dB)	–	26 (0.5λ)	78.26 × 13.2 mm^2 (0.382λ^2)	78.26 × 78.26 mm^2 (2.265λ^2)
[10]	metamaterial-based	2.67	2.37–2.98 (22.8%)	30 dB	2.36–2.82 GHz (19.3%)	21.1 (0.18λ)	13.3 × 16 mm^2 (0.0169λ^2)	100 × 50 mm^2 (0.4λ^2)
[11]	metamaterial-based	2.45	2.1–2.55 (19.4%)	20 dB (improve by 13 dB)	2.43–2.46 GHz (1.2%)	15.3 (0.125λ)	25 × 13 mm^2 (0.0218λ^2)	>38.5 × 39.5 mm^2 (0.4λ^2)
[12]	metamaterial-based	2.42	2.4–2.44 (1.5%)	42 dB (improve by 16 dB)	–	15 (0.122λ)	59 × 20 mm^2 (0.078λ^2)	113 × 113 mm^2 (0.844λ^2)
[13]	DGS (slotted ground)	2.4	2.27–2.35 (3.5%)	20 dB	–	15 (0.115λ)	43 × 10 mm^2 (0.028λ^2)	43 × 43 mm^2 (0.118λ^2)
[16]	T-shaped ground branch	2.45	2.425–2.45 (1%)	30 dB (improve by 25 dB)	2.41–2.47 GHz (2.5%)	3.6 (0.0294λ)	20 × 4.5 mm^2 (0.006λ^2)	40 × 20 mm^2 (0.054λ^2)
[21]	neutralisation line	2	1.8–2.2 (3.5%)	20 dB	–	18 (0.115λ)	18 × 0.5 mm^2 (0.0004λ^2)	100 × 40 mm^2 (0.178λ^2)
proposed	DSPGR	2.45	2.18–2.65 (19.5%)	27.6 dB (improved by 16.6 dB)	2.18–2.65 GHz (19.5%)	16.2 (0.13λ)	16.2 × 10.13 mm^2 (0.01λ^2)	72.4 × 20 mm^2 (0.094λ^2)

λ: free space wavelength; —: cannot found in source.

low mutual coupling without requiring any change in the DSPGR structure. In the following sections, we use $l_3 = 7.5$ mm to set the MIMO antenna to operate in the 2.4-GHz WLAN frequency band which requires a bandwidth from 2.4 to 2.48 GHz.

4.2 S-Parameters

The proposed MIMO antenna has been simulated and measured using the vector network analyzer (VNA) Rohde & Schwarz ZVA 24. Since the antenna has a symmetrical structure, S_{11} and S_{21} are theoretically identical to S_{22} and S_{21}, respectively, so we only show the simulated S_{11} and S_{21}. For measurement, we show all S_{11}, S_{21} (same as S_{12}) and S_{22} results. In measurement, when port #1 is excited, port #2 is terminated with a 50-Ω load, and vice versa. The simulated and measured S-parameters of the MIMO antennas are shown in Fig. 7, where good agreements can be observed. As expected, the measured S_{11} and S_{22} are very similar. The measured IMBW (for S_{11} and $S_{22} \leq -10$ dB) of the antenna is about 2.38–2.51 GHz, which is large enough to cover the WLAN frequency band from 2.4 to 2.48 GHz. In the 2.4-GHz WLAN frequency band, the simulated and measured S_{21} range from −27.2 to −26.3 dB and from −33.5 to −30 dB, respectively.

4.3 Radiation performance

The radiation pattern, efficiency and realised gain of the proposed MIMO antenna have been measured using the antenna measurement equipment Satimo, Starlab system. The simulated and measured radiation patterns of the MIMO antenna at 2.45 GHz in the x–z and y–z planes are shown in Fig. 8. In the study, when port #1 is excited, port #2 is terminated with a 50-Ω load, and vice versa. It can be seen in Fig. 8*a* that IFAs #1 and #2 have nearly omnidirectional patterns in the x–z plane, typical for IFA antenna. In Fig. 8*b*, the radiation patterns of IFAs #1 and #2 are complementary to each other, meaning that the two antenna elements can receive signals from different directions to provide pattern diversity.

The simulated and measured results in efficiency and realised peak gain of the MIMO antenna are shown in Fig. 9. The efficiencies shown include the lost due to antenna mismatching. Since the antenna has a symmetrical structure, the simulated efficiencies and realised peak gains of the two IFA elements, IFAs #1 and #2, are identical. However, due to fabrication and measurement tolerances, the measured efficiencies and realised peak gains of the two IFA elements are not exactly the same. Thus the measured efficiency and realised peak gain shown in Fig. 9 are the average values of the two IFA elements and will be used for discussions. It can be seen that the simulated and measured efficiencies as shown in Fig. 9*a* range from 91–98 to 68.2–73.6%, respectively, in the 2.4-GHz WLAN band (2.4–2.48 GHz). The simulated and measured realised peak gains as shown in Fig. 9*b* range from about from 1.42–1.73 to 1.04–1.39 dBi, respectively, in 2.4-GHz WLAN band. The lower values in the measured results are mainly due to some energy absorbed by the ferrite bead chocks as described previously.

4.4 MIMO performance

The diversity and multiplexing performances of the MIMO antenna are evaluated using ECC and multiplexing efficiency, respectively. ECC measures correlation of signal envelopes and is here used to evaluate correlation of the signals received by the two IFAs elements. Assuming uniform 3D angular-power spectra, the simulated and measured 3D radiation patterns of the MIMO antenna are used in (7) of [27] to calculate the ECC ρ_e and results are shown in Fig. 10*a*. The small discrepancy in ρ_e is due to the difference between using the simulated and measured radiation patterns in calculations. It can be seen that, in the 2.4-GHz WLAN band, the ECC ρ_e using the measured radiation patterns ranges from 0.08 to 0.09 and using the simulated radiation patterns is close to zero (<0.001). These results are significantly less than the widely adopted criterion of ECC < 0.5 for MIMO antennas [28], indicating that the two antenna elements have low correlation and hence good diversity performance.

To evaluate the multiplexing performance of the MIMO antenna, the multiplexing efficiency proposed in [29] is used. Multiplexing efficiency measures the ratio of signal-to-noise ratio (SNR) between imperfect MIMO antenna and ideal antenna in an independent, identically distributed channel to obtain the same system capacity. Under uniform power assumption for a MIMO system with two ideal transmit antennas and two non-ideal receive antennas, the multiplexing efficiency is given by [29]

$$\eta_{\text{mux}} = \sqrt{\eta_1 \eta_2 (1 - |\rho_c|^2)} \tag{1}$$

where η_1 and η_2 are the efficiencies of the non-ideal antennas and ρ_c is the complex correlation coefficient between the two antennas. In Rayleigh fading, the relationship between ρ_c and ρ_e is given by [30]

$$\rho_e \simeq |\rho_c|^2 \tag{2}$$

Therefore substituting (2) into (1) yields

$$\eta_{\text{mux}} \simeq \sqrt{\eta_1 \eta_2 (1 - \rho_e)} \tag{3}$$

Applying the efficiencies of IFAs #1 and #2 shown in Fig. 9*a* and the ECC (ρ_e) in Fig. 10*a* to (3), the calculated multiplexing efficiency is shown in Fig. 10*b*. It can be seen that the measured multiplexing efficiency in the 2.4-GHz WLAN band ranges from 66 to 70.5%, which is acceptable in industry [31].

4.5 Comparison with other designs

Finally, the proposed design using the DSPGR is compared, in terms of centre frequency, IMBW, isolation level, decoupling bandwidth, edge-to-edge antenna spacing, decoupling structure size and total antenna size, with those of other decoupling methods proposed recently [4–6, 8–13, 16, 21] in Table 2. Some of these methods did not have results on efficiencies and MIMO performances such as ECC and multiplexing efficiency, which therefore cannot be compared. It can be seen that, among these designs, the IMBWs of the designs in [4, 10, 11] are 22.6, 22.8, 19.4%, respectively, and are larger than 19.5% of the proposed design. However, the decoupling bandwidth of [4, 11] both are only 1.2%, much smaller than 19.5% of the proposed design. Although the one in [10] has a decoupling bandwidth of 19.3%, slightly smaller than our proposed method (19.5%), it has a distance of 0.18λ between the two antennas and a decoupling structure size of $0.0169\lambda^2$, resulting in a total antenna size of $0.4\lambda^2$. While the proposed antenna has distance of 0.13λ between the two antennas and a decoupling structure size of $0.01\lambda^2$, resulting in a much smaller antenna size of only $0.094\lambda^2$. Thus having considered the IMBW and decoupling bandwidth, the proposed antenna is most compact.

5 Conclusions

A decoupling technique using a DSPGR for a MIMO antenna operating in the WLAN band has been proposed. The antenna consists of two IFA elements as radiators, which are installed on the ground plane with a separated distance of only 16.2 mm (0.13λ). Measured results have shown that the MIMO antenna has an operating bandwidth of 2.38–2.51 GHz, which is large enough to cover the WLAN frequency band from 2.4 to 2.48 GHz, and the DSPGR can significantly reduce mutual coupling to the range of −33.5 to −30 dB within the operating band. The simulated and measured radiation performances in terms of antenna gain, efficiency, radiation patterns, ECC and multiplexing efficiency of the MIMO antenna have also all been studied. Results have indicated that the proposed decoupling technique is very effective in reducing mutual coupling between antenna elements in small MIMO antennas.

6 References

1 Foschini, G.J., Gans, M.J.: 'On limits of wireless communications in a fading environment when using multiple antennas', *Wirel. Pers. Commun.*, 1998, **6**, pp. 311–335
2 Soltani, S., Murch, R.D.: 'A compact planar printed MIMO antenna design', *IEEE Trans. Antennas Propag.*, 2015, **63**, (3), pp. 1140–1149
3 Jensen, M.A., Wallace, J.W.: 'A review of antennas and propagation for MIMO wireless communications', *IEEE Trans. Antennas Propag.*, 2004, **52**, (11), pp. 2810–2824
4 Chen, S.C., Wang, Y.S., Chung, S.J.: 'A decoupling technique for increasing the port isolation between two strongly coupled antennas', *IEEE Trans. Antennas Propag.*, 2008, **56**, (12), pp. 3650–3658
5 Zhao, L.Y., Yeung, L.K., Wu, K.L.: 'A coupled resonator decoupling network for two-element compact antenna arrays in mobile terminals', *IEEE Trans. Antennas Propag.*, 2014, **62**, (5), pp. 2767–2776
6 Coetzee, J.C., Yu, Y.T.: 'Port decoupling for small arrays by means of an eigenmode feed network', *IEEE Trans. Antennas Propag.*, 2008, **56**, (6), pp. 1587–1593
7 Lin, K.C., Wu, C.H., Lai, C.H., *et al.*: 'Novel dual-band decoupling network for two-element closely spaced array using synthesized microstrip lines', *IEEE Trans. Antennas Propag.*, 2012, **60**, (11), pp. 5118–5128
8 Yang, F., Rahmat-Samii, Y.: 'Microstrip antennas integrated with electromagnetic band-gap (EBG) structures: a low mutual coupling design for array application', *IEEE Trans. Antennas Propag.*, 2003, **51**, (10), pp. 2936–2946
9 Farahani, H.S., Veysi, M., Kamyab, M., *et al.*: 'Mutual coupling reduction in patch antenna arrays using a UC-EBG superstrate', *IEEE Antennas Wirel. Propag. Lett.*, 2010, **9**, pp. 57–59
10 Hsu, C.C., Lin, K.H., Su, H.L.: 'Implementation of broadband isolator using metamaterial-inspired resonators and a T-shaped branch for MIMO antennas', *IEEE Trans. Antennas Propag.*, 2011, **59**, (10), pp. 3936–3939
11 Ketzaki, D.A., Yioultsis, T.V.: 'Metamaterial-based design of planar compact MIMO monopoles', *IEEE Trans. Antennas Propag.*, 2013, **61**, (5), pp. 2758–2766
12 Zhai, G.H., Chen, Z.N., Qing, X.M.: 'Enhanced isolation of a closely spaced four-element MIMO antenna system using metamaterial mushroom', *IEEE Trans. Antennas Propag.*, 2015, **63**, (8), pp. 3362–3370
13 Chiu, C.Y., Cheng, C.H., Murch, R.D., *et al.*: 'Reduction of mutual coupling between closely-packed antenna elements', *IEEE Trans. Antennas Propag.*, 2007, **55**, (6), pp. 1732–1738
14 Ouyang, J., Yang, F., Wang, Z.M.: 'Reducing mutual coupling of closely spaced microstrip MIMO antennas for WLAN application', *IEEE Antennas Wirel. Propag. Lett.*, 2011, **10**, pp. 310–313
15 Wu, D., Cheung, S.W., Yuk, T.I., *et al.*: 'Design of a printed multiband MIMO antenna'. 2013 Seventh European Conf. on Antennas and Propagation (EuCAP), 2013, pp. 2020–2023
16 Mak, A.C.K., Rowell, C.R., Murch, R.D.: 'Isolation enhancement between two closely packed antennas', *IEEE Trans. Antennas Propag.*, 2008, **56**, (11), pp. 3411–3419
17 Lau, B.K., Andersen, J.B.: 'Simple and efficient decoupling of compact arrays with parasitic scatterers', *IEEE Trans. Antennas Propag.*, 2012, **60**, (2), pp. 464–472
18 Ban, Y.L., Yang, S., Chen, Z., *et al.*: 'Decoupled planar WWAN antennas with T-Shaped protruded ground for smartphone applications', *IEEE Antennas Wirel. Propag. Lett.*, 2014, **13**, pp. 483–486
19 Liu, L., Cheung, S.W., Yuk, T.I.: 'Compact MIMO antenna for portable devices in UWB applications', *IEEE Trans. Antennas Propag.*, 2013, **61**, (8), pp. 4257–4264
20 Liu, L., Cheung, S.W., Yuk, T.I.: 'Compact multiple-input–multiple-output antenna using quasi-self-complementary antenna structures for ultrawideband applications', *IET Microw. Antennas Propag.*, 2014, **8**, (13), pp. 1021–1029
21 Diallo, A., Luxey, C., Thuc, P.L., *et al.*: 'Study and reduction of the mutual coupling between two mobile phone PIFAs operating in the DCS1800 and UMTS bands', *IEEE Trans. Antennas Propag.*, 2006, **54**, (11), pp. 3063–3074
22 Diallo, A., Luxey, C., Thuc, P.L., *et al.*: 'Enhanced two-antenna structures for universal mobile telecommunications system diversity terminals', *IET Microw. Antennas Propag.*, 2008, **2**, (1), pp. 93–101
23 Huang, S.Y., Lee, Y.H.: 'A compact E-Shaped patterned ground structure and its applications to tunable bandstop resonator', *IEEE Trans. Microw. Theory Tech.*, 2009, **57**, (3), pp. 657–666
24 Xue, Q., Shum, K.M., Chan, C.H.: 'Novel 1-D microstrip PBG cells', *IEEE Microw. Wirel. Compon. Lett.*, 2000, **10**, pp. 403–405
25 Cheung, S.W., Wu, D., Liu, L., *et al.*: 'Isolation improvement using CMRC for MIMO antennas'. 2015 Ninth European Conf. on Antennas and Propagation (EuCAP), Lisbon, 2015, pp. 1–4
26 Zhang, Z.J.: 'Antenna design for mobile devices' (John Wiley & Sons, Singapore, 2011)
27 Knudsen, M.B., Pedersen, G.F.: 'Spherical outdoor to indoor power spectrum model at the mobile terminal', *IEEE J. Sel. Areas Commun.*, 2002, **20**, (6), pp. 1156–1169
28 Vaughan, R.G., Andersen, J.B.: 'Antenna diversity in mobile communications', *IEEE Trans. Veh. Technol.*, 1987, **36**, (4), pp. 149–172
29 Tian, R., Lau, B.K., Ying, Z.N.: 'Multiplexing efficiency of MIMO antennas', *IEEE Antennas Wirel. Propag. Lett.*, 2011, **11**, pp. 183–186
30 Clarke, R.H.: 'A statistical theory of mobile radio reception', *Bell Syst. Techn. J.*, 1966, pp. 957–1000
31 Zhang, S., Glazunov, A.A., Ying, Z.N., *et al.*: 'Reduction of the envelope correlation coefficient with improved total efficiency for mobile LTE MIMO antenna arrays: mutual scattering mode', *IEEE Trans. Antennas Propag.*, 2013, **61**, (6), pp. 3280–3291